Nat Hazards
DOI 10.1007/s11069-014-1120-9

ORIGINAL PAPER

The sun-hurricane connection: Diagnosing the solar impacts on hurricane frequency over the North Atlantic basin using a space–time model

Robert E. Hodges · Thomas H. Jagger · James B. Elsner

Received: 13 December 2013 / Accepted: 1 March 2014

Abstract The authors define a spatio-statistical response of hurricane frequency to the solar cycle. Previous research indicates reduced (increased) hurricane intensities and frequency in the western (eastern) tropical Atlantic. However, no formal quantitative relationship has been spatially established between hurricane frequency and solar activity. The authors use a Bayesian hierarchical space–time model, an increasingly popular approach due to its advantage in facilitating regression modeling of space–time phenomena in the context of large data sets. Regional hurricane frequency over the period 1866–2010 is examined in response to September sunspot number (SSN) while controlling for other relevant climate factors. The response features a 13 % reduction in probability of annual hurricane occurrence for southeastern Cuba, the southern Bahama islands, Haiti, and Jamaica when the SSN is 80 sunspots. In contrast, hurricane risk in regions of the southeastern Atlantic is predicted to increase by 73 % when the SSN is 160 sunspots. The model can be ported to explore other relationships over contiguous space.

Keywords Sunspots · Hurricanes · North Atlantic Oscillation · El Niño Southern Oscillation · Sea-surface temperatures · Risk · Bayesian · Space–time model · Hexagon tessellation

1 Introduction

North Atlantic hurricanes are severe tropical cyclones characterized by heavy rain, winds, and extremely low surface pressures. With maximum sustained winds of at least 33 ms^{-1}, they constitute a major problem for much of the basin's shoreline. Observed increases in coastal population serve only to exacerbate the hurricane risk to life and property.

R. E. Hodges (✉) · T. H. Jagger · J. B. Elsner
Department of Geography, Florida State University, Tallahassee, FL, USA
e-mail: rehodges@fsu.edu

Published online: 21 March 2014

Hurricanes are driven by the flow of heat and moisture from the ocean surface to the overlying atmosphere. The warm seas found in tropical low-latitudes provide nearly continuous heat and moisture fluxes into near-surface air. Traditionally, the sun's role in hurricane climate studies is thought of as a simple variable governing ocean heat content and the calendar date as a predictor of tropical cyclone frequency and intensity. But the sun features low- and high-amplitude modulations in energy output that can also influence hurricane activity.

The idea of a connection between solar activity and hurricanes extends back to the nineteenth century Meldrum (1872), Poey (1873), through the twentieth century Visher (1924), Willett (1951), Cohen and Sweetser (1975) and into the twenty-first century Elsner and Jagger (2008), Elsner et al. (2010), Hodges and Elsner (2012).

Variations in solar activity are monitored by sunspots. Sunspots are visible disturbances on the photosphere of the sun. During the sun's 11-year (on average) geographic switching of magnetic poles, dark central cores (*umbra*) appear in various shapes (*penumbra*) in response to the convective inhibition of solar plasma induced by migrating magnetic fields Weiss (2007). The cooler, darker sunspots decrease overall solar luminosity. However, cloud-like features (*faculae*) above the sunspot are roughly 300 K higher than the normal surface temperature of the sun of 5,778 K, an increase of 5.2 %. The result is higher overall solar irradiance, especially in the ultraviolet and extreme ultraviolet wavelengths as described by Planck's law. Earth's stratospheric ozone absorbs this additional UV energy, and the result is increased stratospheric and upper-tropospheric temperatures Labitzke et al. (2002), Hood (2003).

Elsner and Jagger (2008)—hereafter, EJ08—report fewer intense hurricanes over the Caribbean and Gulf of Mexico when sunspots are high. The finding is inline with the heat-engine theory of hurricanes Emanuel (1987), which predicts a reduction in the maximum potential intensity in response to warming in the atmospheric layer near the top of the hurricane. Recent work by Emanuel et al. (2013) reports that the 1979–2010 observed increase in potential intensity is a result of tropical tropopause cooling, outpacing the thermodynamic contribution from warming seas by a factor of eight. This supports Elsner et al. (2010) findings where quantile regression revealed that high solar activity over the western Caribbean leads to a -4.3 ± 1.86 ms^{-1} mean reduction in daily maximum wind speed and a 90th percentile storm wind reduction of almost 9 ms^{-1} per 0.01 Mg II core-to-wing ratio units (SD), another measure of solar UV forcing.

However, EJ08 also note that high numbers of sunspots correspond with higher intensities in the eastern tropical Atlantic. The geographic difference is speculated as the result in limiting factors for potential intensity. The western tropical Atlantic features higher SST than the eastern tropical Atlantic, rendering the upper-tropospheric warming from increased solar activity the limiting factor in the west. The eastern tropical Atlantic demonstrates warmer sea-surface temperatures when the sun is active White et al. (1997), Elsner et al. (2008). Nevertheless, a spatially heterogenous response in hurricane intensity and frequency is observed in response to changes in solar activity.

Hodges and Elsner (2012) — hereafter, HE12—describe the spatial response of hurricanes to extremes in the solar cycle using descriptive statistics. Regional hurricane frequency from 1851 to 2010 indicates fewer hurricanes across the Caribbean and along the eastern seaboard of the USAwhen sunspots are numerous. In contrast, fewer hurricanes are observed in the central and eastern North Atlantic when sunspots are few. Remarkably, solar cycles are as important toward describing regional hurricane frequency as the El Niño Southern Oscillation, one of the most important sources of hurricane variability in the North Atlantic Arkin (1982), Gray (1984).

Needed is a more formal quantification of the sun-hurricane connection. The purpose of this treatment is to assess the statistical relationship between solar activity and hurricane

activity over the North Atlantic at a finer, regional scale. A hierarchical space–time model is applied toward this end.

The data used in this study are introduced in Sect. 2. In Sect. 3, the construction of the equal-area hexagon grid is described. Also in this section, the space–time model construction and implementation are described. Model results are presented in Sect. 4, followed by a discussion in Sect. 5. A summary of the work is presented in Sect. 6.

2 Data

The best-track data set contains the six-hourly center locations and intensities of all known tropical cyclones across the North Atlantic basin, including the Gulf of Mexico and Caribbean Sea. The data set is called HURDAT (HURricane DATa). It is maintained by the US National Oceanic and Atmospheric Administration at the National Hurricane Center. Tropical cyclone center locations are given in geographic coordinates (in tenths of degrees). The intensities, representing the 1-min near-surface ($\approx$10 m) wind speeds, are given in knots (1 kt = 0.5144 ms^{-1}). The minimum central pressures are given in millibars (1 mb = 1 hPa). The data are provided in six-hourly intervals starting at 00 Universal Time Coordinate (UTC). The version of HURDAT used here contains data through 2010. Updated information is available online (www.nhc.noaa.gov/pastall.shtml#hurdat). Information on the history and origin of these data are found in Jarvinen et al. (1984).

For each cyclone, the HURDAT observations are 6 h apart. For spatial analysis and modeling, this can be too coarse, as the average forward motion of hurricanes is 6 ms^{-1} (12 kt). Therefore, the data are imputed using interpolation to 1 h. Wind speeds are smoothed using a third-degree polynomial, capturing most of the fluctuation in cyclone intensity without over-fitting to the random variations and consistent with the 5-kt precision of the raw wind speed Jagger and Elsner (2006).

Solar activity will be described via monthly mean International sunspot numbers as made available by the National Geographic Data Center. It was originally constructed by Solar Influences Data Analysis Center, World Data Center at the Royal Observatory of Belgium. Reliable monthly observations extend back to 1749. Swiss astronomer Johann Rudolph Wolf introduced a daily measurement technique that observes both total spots observed and the quantity of their clusterings. The data set addresses observed error by incorporating a weighted average of cooperating observations.

Pertinent to this study is the sunspot numbers for September, the peak month of the North Atlantic hurricane season. Identified by EJ08 and spatially investigated in HE12, September sunspots (SSN) are associated with decreased (increased) US (east and central Atlantic) hurricanes. For the 145-year study period used here from 1866–2010, the range of SSN is between 0.6 sunspots and 235.8 sunspots, with mean 56.5 sunspots and median 48.1 sunspots (Fig. 1a).

The North Atlantic Oscillation (NAO) index is the monthly difference in normalized sea-level pressures between Stykkisholmur, Iceland and Ponta Delgada, Azores. It is an important pattern of global interannual variability Hurrell and Loon (1997), Mann and Park (1994). May–June annual averages of the NAO index are used to identify the steering effects of the subtropical high on hurricanes. The selection is a trade-off between the maximum signal that occurs during boreal winter and the proximity to the month of September, the peak of the North Atlantic hurricane season Elsner and Kocher (2000). The 145-year range of the NAO index is between -2.76 and 2.90 units of SD, with mean -0.36 units and median -0.43 units (Fig. 1b).

The El Niño Southern Oscillation (ENSO) is a coupled ocean-atmospheric phenomenon whose impact on hurricanes has been well established. The Southern Oscillation Index (SOI) anomalies represent the normalized air pressure difference between Darwin and Tahiti. The change in equatorial Pacific SST leads to an atmospheric pressure imbalance whose far-reaching effects produce wind shear in the North Atlantic Main Development Region during El Niño phases. Monthly values of the SOI anomalies are obtained from the UK Climatic Research Unit (http://www.cru.uea.ac.uk/cru/data/soi/). For technical descriptions of the SOI anomalies data, see Allan et al. (1991), Können et al. (1998), Ropelewski and Jones (1987). SOI anomalies data begin January 1866. Annual averages of August–October SOI values are used as an indicator of shear upon North Atlantic hurricanes Elsner and Jagger (2008), Hodges and Elsner (2012). The 145-year range of the SOI is between −6.67 and 8.07 units of SD, with mean −0.26 units and median −0.27 units (Fig. 1c).

Sea-surface temperatures (SST) are a critical component for tropical cyclogenesis and intensification. Hurricanes, previously described as giant heat engines, make use of tropical oceans as a continual source of moisture and heat to sustain the release of latent heat from condensation which powers its warm core. Higher SST, all else being equal, should provide a more conducive environment for tropical cyclone development. However, the spatial patterns of SST are not homogeneous. Therefore, regional SST information is useful. SST data used here come from NOAAs Extended Reconstructed Sea Surface Temperature (version 3b) at 2° resolution, provided by the NOAA Smith et al. (2008), specifically NOAA/OAR/ESRL PSD in Boulder, Colorado (http://www.esrl.noaa.gov/psd/).

3 Methods

3.1 Spatial grid

Using the procedure outlined in Elsner et al. (2011) and employed in HE12, we create an equal-area ($\approx$519,950 km^2) hexagon tessellation to examine North Atlantic hurricanes by region. The number of hurricanes that passes through a given region per year is recorded once, regardless of how many observations reside in the region. The result is an annual count and average per year of hurricanes (Fig. 2). The range in counts for all regions from 1866 to 2010 is 1 and 176 hurricanes. The range in hurricane frequency per year for all regions is 0.01 and 1.21.

SST data points are also captured per region, ranging from 2 to 16 SST observations collected per region. Observations are then averaged. To facilitate modeling, the 145-year mean regional mean is assessed and removed. The result is a regional SST anomaly. Regional anomalies range between −2.60 and 2.43 °C, with mean and median 0 °C. Figure 3 displays the SST time series.

3.2 Space–time model

Having constructed a spatial framework, we now proceed to developing a statistical model capable of assessing the impacts of solar activity. However, other factors are known to affect hurricanes in the North Atlantic, such as the ENSO, the NAO, SST, and observation issues prior to the advent of satellite coverage. Therefore, the model should account for these concurrently with solar activity. A multiple regression model can describe the marginal contributions of individual predictors on an outcome variable such as regional hurricane frequency (Fig. 4).

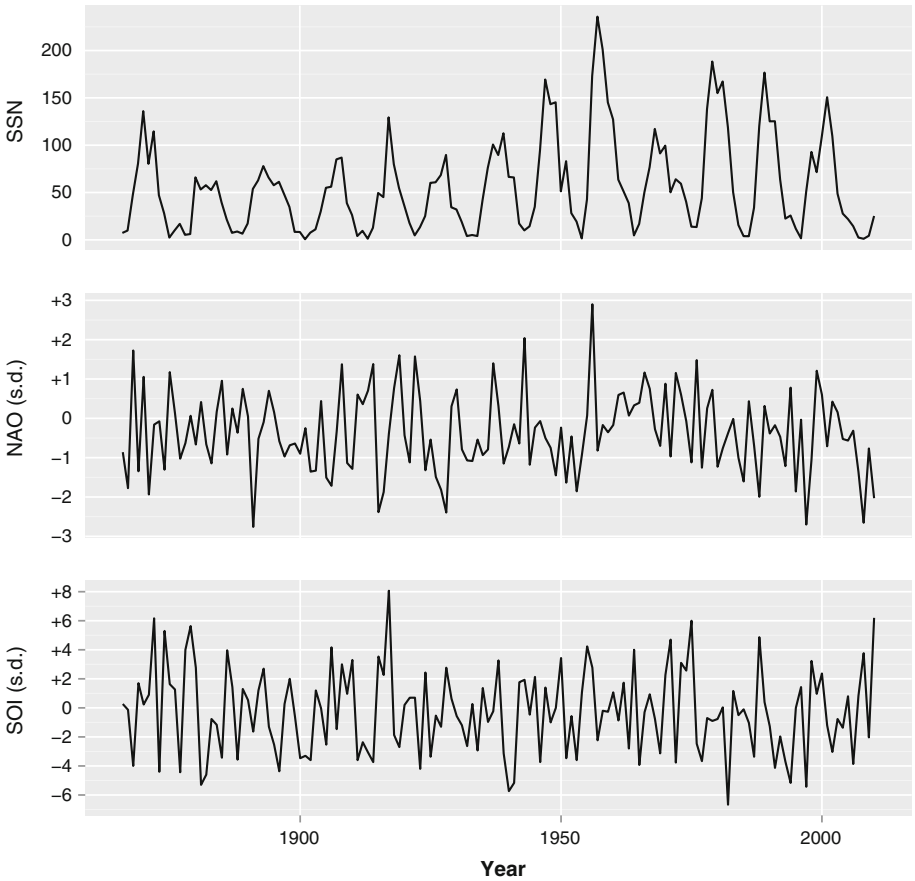

Fig. 1 Time series of (a) September sunspots (SSN), (b) May–June averaged North Atlantic Oscillation (NAO) units, and (c) August–October averaged Southern Oscillation Index (SOI) units for the period 1866–2010.

Other factors to consider include the rare count nature of regional hurricane counts per year, which requires use of a generalized linear model. We employ a Poisson model that uses the logarithm of the dependent variable as the canonical link function to a linear regression of the covariates.

Another complicating factor is the presence of spatial autocorrelation in annual hurricane frequency over the hexagon tessellation (Fig. 2). The dependency arises from the movement pattern of hurricanes over the domain in a given season. A hurricane counted in one hexagon region will likely possess at least one neighbor that also observed that hurricane. The result is a spatial dependence in the hurricane counts. Accordingly, we use a space–time model that accounts for the spatial autocorrelation in hurricane frequency within the gridded domain.

A Bayesian hierarchical model is capable of handling the above-mentioned factors and correspondingly high dimensionality of prescribed data. Using Bayesian inference, a series (or hierarchy) of conditional models are linked together formally via basic probability relationships Wikle and Anderson (2003). The general hierarchical model consists of three

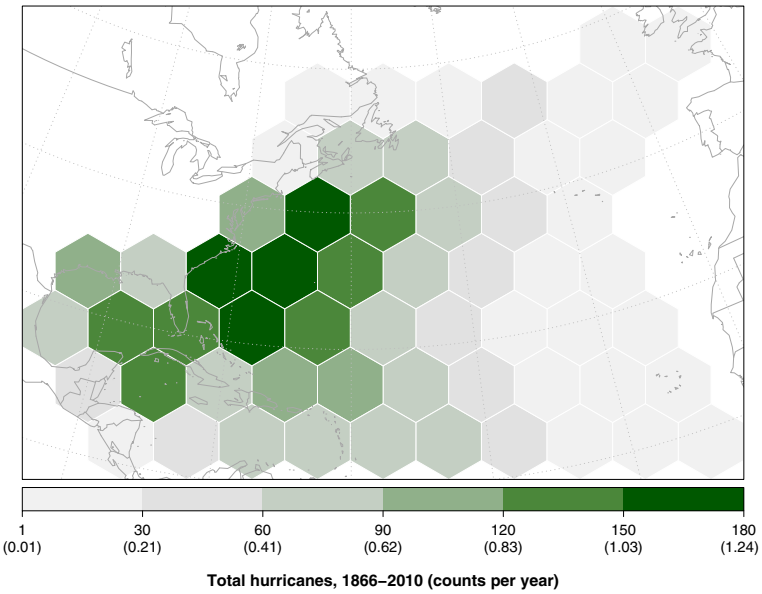

Fig. 2 Total hurricanes and corresponding counts per year for the period 1866–2010. A total of 59 hexagon regions are displayed.

stages: (1) a data model, which describes the probability distribution of the data observations conditional on some process of interest and parameters that describe the data model; (2) a process model, which describes the probability distribution of some underlying process conditional on other parameters; and (3) a parameter model, which describes the probability distribution of the parameters themselves Berliner (1996), Wikle et al. (1998).

3.2.1 Data model

The data model of our spatiotemporal process assumes that the yearly hurricane counts in each region are independent Poisson random variables when conditioned on the underlying Poisson rate process. Formally,

$$H_{s,t} \sim \text{ dpois } (\lambda_{s,t}) \tag{1}$$

where $H_{s,t}$ represents hurricane counts and $\lambda_{s,t}$ represents the underlying Poisson rate, in hexagon regions s = 1,…, S representing hexagon regions 1 through 59 at times t = 1,…, T representing years 1866 through 2010.

3.2.2 Process model

The process model fleshes out the spatiotemporal process impacting regional hurricane frequency using a multivariate regression model. Climatological variables known to affect North Atlantic hurricanes are specified here: SSN, SST, SOI, NAO, and an indicator variable given a value of 0 for years 1866–1965 and a value of 1 for years 1966–2010 to address likely hurricane undercounts in the eastern Atlantic prior to satellite coverage

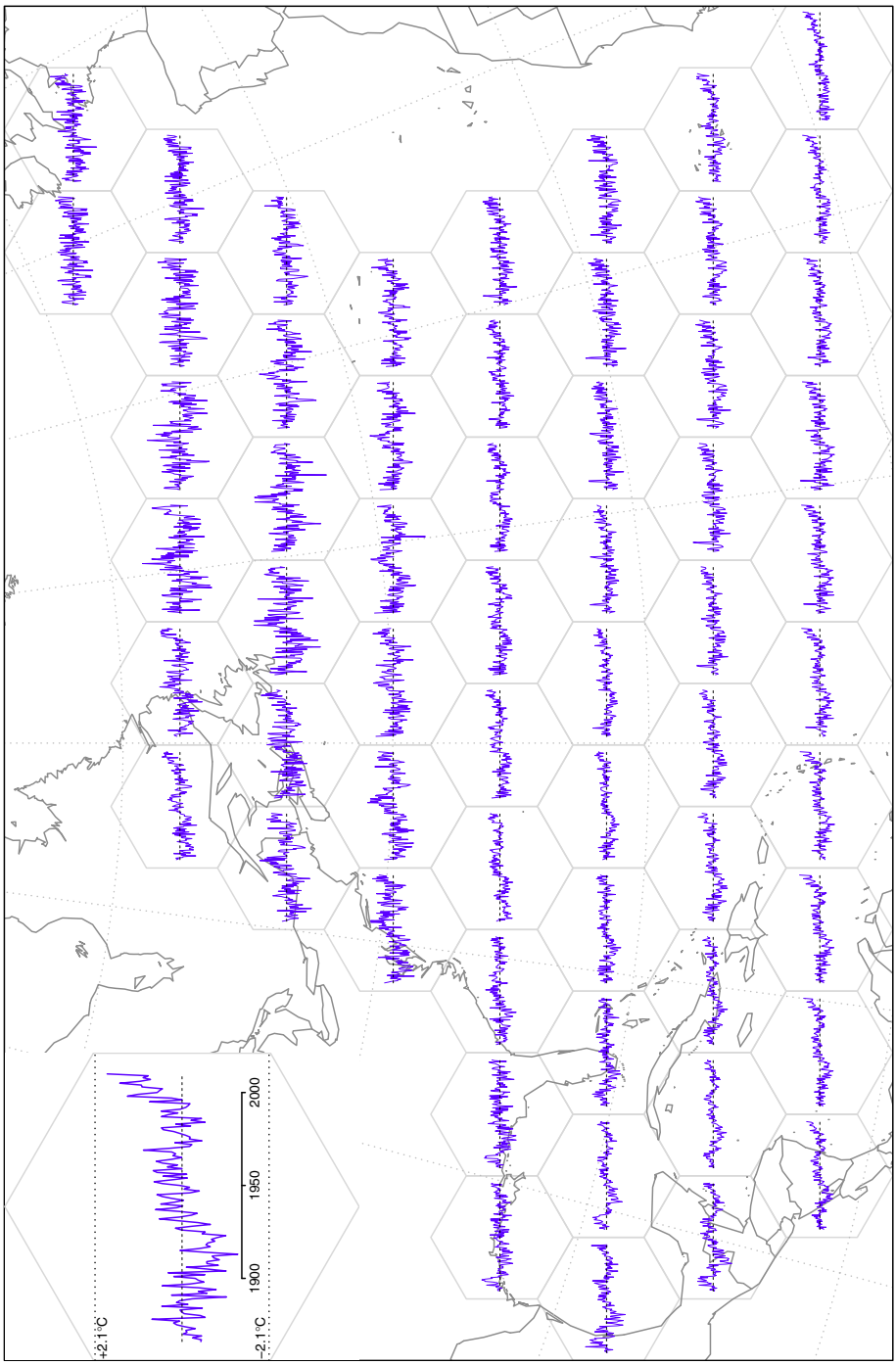

Fig. 3 Sea-surface temperature anomalies (SST) from 1866–2010. A regional maximum of +2.43 °C is found in the region northeast to that containing the tip of Newfoundland and a regional minimum of −2.60 °C directly to the southeast of the regional maximum.

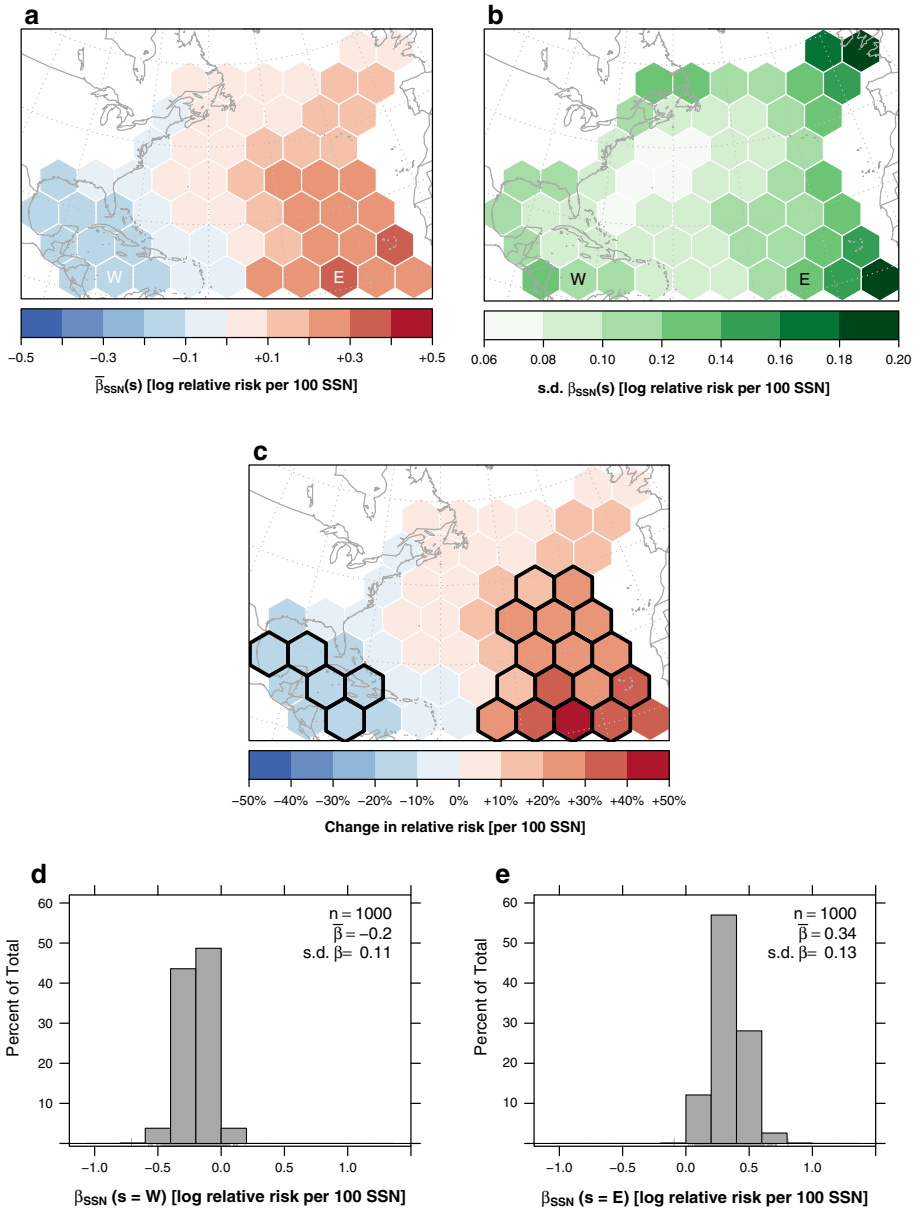

Fig. 4 Space–time model output for September sunspot number (SSN). (a) Regional mean change in log relative risk (β_{SSN}) of hurricane frequency per region per 100 SSN. (b) Same, but for the SD. (c) Regional change in relative risk (β_{SSN}) of hurricane frequency per 100 SSN, conditional upon holding all other covariates constant. Positive values (*red*) indicate regions where fewer storms are predicted when SSN is low. Negative values (*blue*) indicate regions where fewer storms are predicted when SSN is high. Hexagon regions where <10 % of β_{SSN} samples are below (or above) zero are outlined in *black*. (d) Histogram of β_{SSN} for region W. (e) Same, but for region E.

(SAT) starting in 1966 Neumann et al. (1999). We model the logarithm of the Poisson rate as a linear combination of the predictors. Formally,

$$\log(\lambda_{s,t}) = \beta_{\mathrm{SST}}(s) \cdot \mathrm{SST}_{s,t} + \beta_{\mathrm{SSN}}(s) \cdot \mathrm{SSN}_{t} + \beta_{\mathrm{SOI}}(s) \cdot \mathrm{SOI}_{t} + \beta_{\mathrm{NAO}}(s) \cdot \mathrm{NAO}_{t} + \beta_{\mathrm{SAT}}(s) \cdot \mathrm{SAT}_{t} + \eta(s), \quad (2)$$

where $\beta_{\mathrm{SST}}(s)$ are regional regression coefficients for SST that vary by region and year, the remaining $\beta(s)$ terms are regional regression coefficients for SSN, SOI, NAO and SAT that vary by year only, and $\eta(s)$ is the regional error term.

3.2.3 Parameter model

The parameter model addresses uncertainty in the data and process models by assigning them prior distributions. Spatial autocorrelation is accounted for in this stage. We allow the regression coefficients to vary regionally and to be informed by their immediate—and up to a maximum of six—neighboring region values. We assume then that the prior for each spatially varying regression coefficient is the independent sum of unstructured and spatial random effects. Formally, the parameter model is given by

$$\beta_k = U_k + S_k \quad (3)$$

$$U_k \sim N(q_k, I/\tau_{u,k}) \quad (4)$$

$$S_k \sim ICAR(W, \tau_{s,k}). \quad (5)$$

In Eq. 3, β_k is the regression coefficient vector, with components $\beta_k(s)$ where k corresponds to the sequence of SST, SSN, SOI, NAO, and SAT predictors applied per hexagon region (s) plus an intercept term (β_0).

In Eq. 4, $U_k$is the unstructured random effects vector which has a multivariate Normal random distribution with mean q_k and covariance matrix $I/\tau_{u,k}$. That is, $\beta_k(s)$ is a series of i.i.d. normal random variables with mean q_k and variance $I/\tau_{u,k}$. There are six separate values for τ (i.e., the five covariates and one error term) which come from a gamma distribution with a shape of 0.5. The rate parameter is 0.005 for the error term and 0.005 divided by the data variance of the covariates (i.e., 0.005/0.25, 0.005/2485, 0.005/8.6, 0.005/1.1, 0.005/0.21, respectively). These specifications are consistent with the concept of uninformative (or flat) priors, where little information is provided *a priori* to the stochastic calculation.

In Eq. 5, S_k is the spatial random effects vector, which follows an ICAR distribution with weight matrix W and precision $\tau_{s,k}$. The six values of τ used in the spatial component also come from a gamma distribution with a shape of 0.5. The rate parameter is 0.005 for the error term and 0.005 divided by the data variance of the covariates (i.e., 0.005/0.25, 0.005/2485, 0.005/8.6, 0.005/1.1, 0.005/0.21, respectively). The ICAR specification is appropriate for situations of first-order (i.e., direct neighbor) dependency [Shekhar and Xiong (2008) p. 1103] as used here. This specification was first used in Bayesian image restoration Besag et al. (1991). Note that for the ICAR distribution the spatial random effects prior for each component is constrained to sum to zero, so that an intercept term must be used with a flat prior. Here, the intercept is given as q_k, the vector of means for the unstructured component.

The model selection was based on using the model output deviance information criterion (DIC) provided as output by the OpenBugs software. The smallest DIC was produced by the above-listed set of predictors.

3.3 Implementation

We simulate from the posterior distribution using Markov Chain Monte Carlo (MCMC) methods. Specifically, the Gibbs sampler is a special case of Metropolis-Hasting algorithm where unknown parameters are estimated one at a time and conditional upon all the other parameters. The sampled draws are dependent on the previous iteration's values toward arriving at the target posterior distribution [Gelman and Hill (2007) p.397–408]. See §17.8 of Gelman and Hill (2007) for peer-reviewed literature on the Gibbs sampler.

The model is carried out using the Bayesian inference using Gibbs sampler (BUGS) software. BUGS performs Bayesian analysis of many types of statistical models using MCMC methods Gilks et al. (1996). The BUGS code follows the structure demonstrated in §12.4.4 of Elsner and Jagger (2013).

Convergence and mixing diagnostics are performed on the model samples before using them for inference. High values for the precision terms ($\tau = 100$) were assigned to ensure realistic sample values of the uninitialized parameters. To diagnose model convergence and mixing, q_k is initialized with values 0.5 and 1.0, resulting in the construction of two different MCMC chains.

Gelman and Rubin's convergence diagnostic Gelman and Rubin (1992) were used to indicate the potential scale reduction factor (PSRF) between the two chains per covariate per hexagon region after 5,000 samples. PSRF is calculated by comparing the mean and the variance of each chain to the mean and variance of the combined or pooled chain.

SST, SSN, NAO, and SAT covariates produced a maximum PSRF of 1.01 in hexagon regions 18, 22, 50, and 19, respectively (hexagon regions are numbered 1 through 59 and are mapped from left to right, bottom to top). SOI produced a maximum PSRF of 1.0. Values above 1.1 for any parameter would indicate lack of convergence [Gelman and Hill (2007) p. 352], though none qualify. This is evidence that the two model chains—starting from two different points in parameter space—have converged prior to the 5,000th iteration.

The evolution of PSRF over successive model iterations is also important to examine. In effect, it is a visual representation of model chain convergence, and an indicator of how many samples to ignore as part of the model "burn-in." Figure 9 shows the evolution of the PSRF for all covariates for hexagon regions that required the most iterations for convergence. β_{SAT}'s in hexagon region 58 required 1,100 iterations to fall below the 1.1 value threshold. Conservatively, therefore, the first 1,100 samples of the final model will be discarded.

Since the two model chains demonstrate convergence, the second chain ($q_k = 1.0$) is discarded in favor of the first. The first chain ($q_k = 0.5$) is used to diagnose mixing.

Finding the lowest effective sample size among the covariates and hexagon regions will give let us conservatively the number of iterations to thin to repeatedly discard in the final model run. The effective sample size of a model chain is the total number of samples after adjusting for autocorrelation between model iterations Plummer et al. (2006).

For a sequence of 5,000 β_k samples, the SE of the mean is the variance of β_k samples divided by the effective sample size n. The effective sample size is determined by estimating the spectral density at frequency zero. The result is an estimate of how many samples are independent for a given covariate in a given region and, thus, a measure of decay. A higher effective sample size indicates good mixing; a lower effective sample size indicates substantial autocorrelation.

The lowest effective sample size for β_{SST} was 661 in hexagon region 19. For β_{SSN}, 485 samples were produced in hexagon region 30. For β_{SOI}, 976 samples were produced in hexagon region 57. For β_{NAO}, 454 samples were produced in hexagon region 57. For β_{SAT}, 553 samples were produced in hexagon region 44. Using the β_{NAO} effective sample size, we record only the

11th iteration in the final model. Therefore, after a burn-in of 1,100 samples, only the 11th iteration of 11,000 samples is retained in order to produce 1,000 independent samples.

The total number of iterations in the final model is 12,101, which took approximately 1.5 h to complete on a mid-2009 Macbook Pro (2.66 GHz dual-core Intel Xeon processor, 4 Gb of 1067 MHz DDR3 RAM, 1.07 GHz front-side bus speed) running OpenBUGS via WINE on OS X version 10.8.2.

4 Results

For each model covariate, spatial summaries of their respective 1,000 regression coefficients (β_k) samples are displayed in Figs. 5, 6, 7, 8, 9. They include descriptive statistics on the mean and SD of these posterior samples per region. The log relative risk of annual hurricane frequency changes by the respective regression coefficient per covariate unit, given all other covariates are held constant. Histograms on β_k are displayed for select western (W) and eastern (E) regions. This serves as a visualization of the raw space–time model output.

Of climatologic interest are regional relative risk plots. They reflect the percent-change in the rate of annual hurricane frequency given a one unit increase in the covariate, given all other covariates are held constant. They are calculated as

$$[e^{\bar{\beta}_k}(s) - 1] \times 100\%, \tag{6}$$

where $\bar{\beta}_k(s)$ is the regional mean regression coefficient.

We identify grids where <10 % of the posterior samples are below (or above) zero with a black border. These regions indicate where the relationship is likely not due to chance (at the 90 % level).

4.1 September sunspots

Log relative risks of annual hurricane frequency (Fig. 4a) range between −0.20 and +0.34 per 100 SSN throughout the basin. These values also correspond to Fig. 4d and e, regions located in the southwestern Caribbean and southeast tropical Atlantic, respectively.

Relative risks range between −17.8 and +40.9 % (Fig. 4c). The average relative risk over the five significantly negative Caribbean regions is −16.6 % with SD 1.3 %. The average relative risk over the sixteen significantly positive central Atlantic regions is +26.9 % (SD 6.1 %).

4.2 SST

Log relative risks of annual hurricane frequency (Fig. 5a) range between −0.45 and +1.05 per °C over the basin. Values for Figs. 5d and e, regions located in the southwestern Caribbean and southeast tropical Atlantic, are −0.36 and +1.05, respectively.

Relative risks range between −36.4 and +187.1 % (Fig. 5c) over the basin. The average relative risk over the five significantly negative regions is −27.1 % with SD 6.8 %. The average relative risk over the sixteen significantly positive southeast Atlantic regions is +109.1 % (SD 41.1 %).

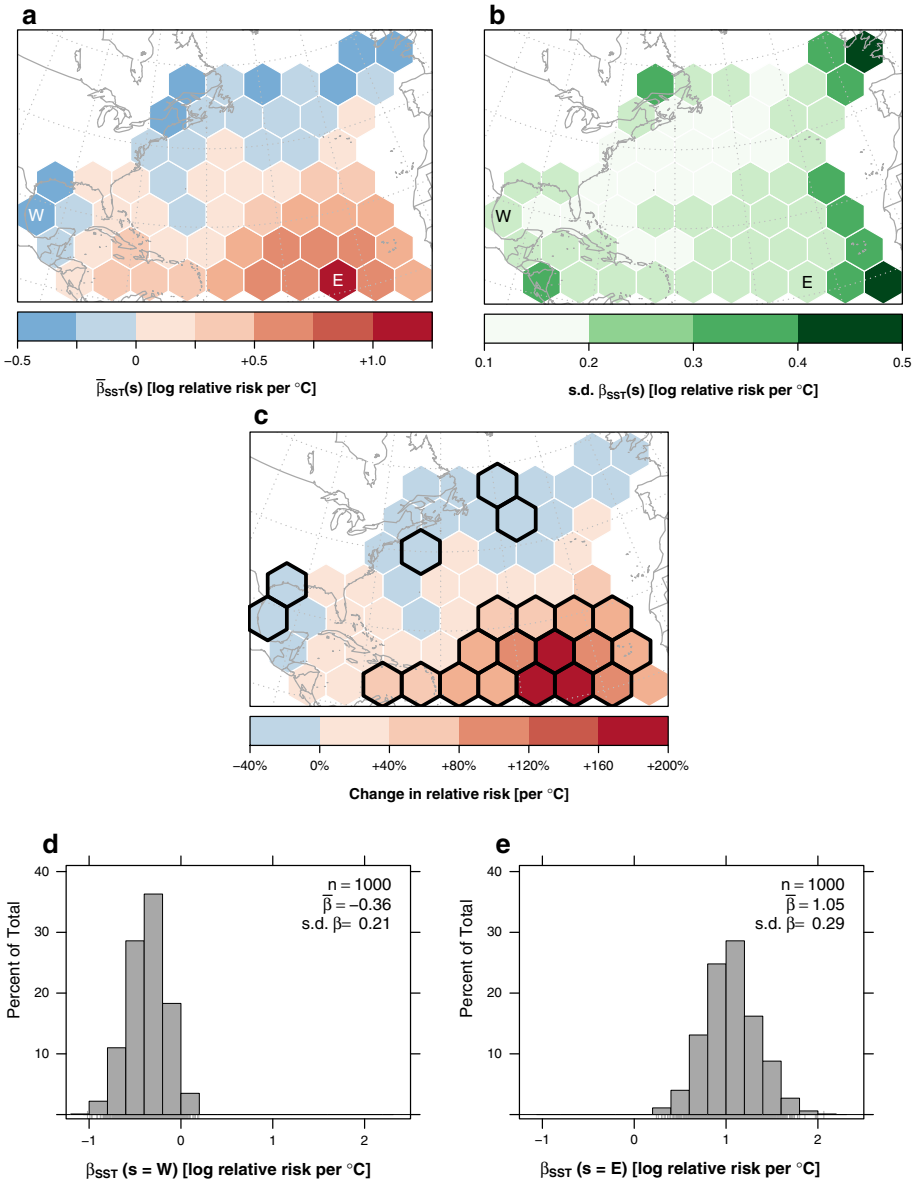

Fig. 5 Space–time model output for sea-surface temperature anomalies (SST). (a) Regional mean change in log relative risk [$\beta_{SST}(s)$] of hurricane frequency per °C. (b) Same, but for the SD. (c) Regional change in relative risk (β_{SSN}) of hurricane frequency per °C increase in SST, conditional upon holding all other covariates constant. Positive values (*red*) indicate regions where more storms are predicted when SST is positive. Negative values (*blue*) indicate regions where more storms are predicted when SST is negative. Hexagon regions where <10 % of β_{SST} samples are below (or above) zero are outlined in *black*. (d) Histogram of β_{SST} for region W. (e) The same, but for region E.

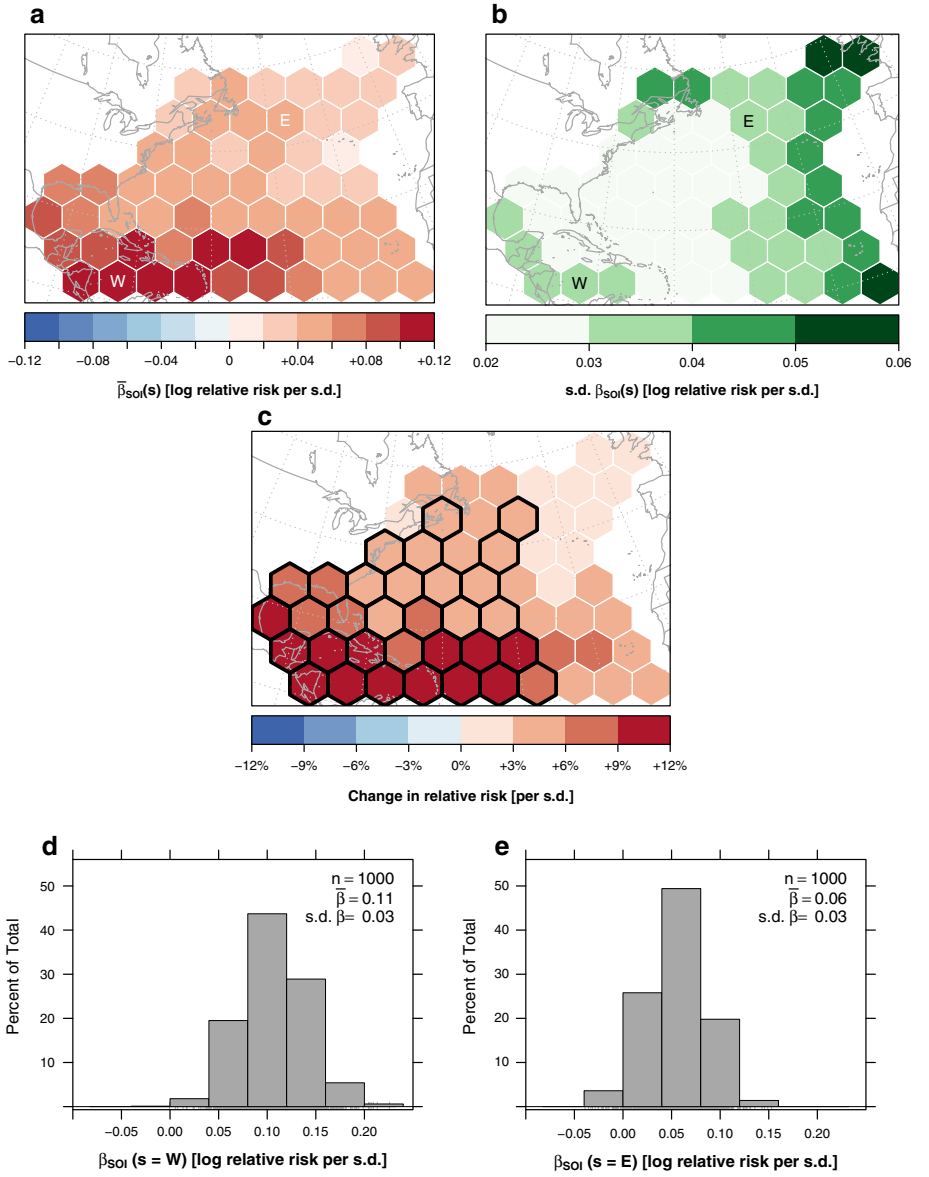

Fig. 6 Space–time model output for the Southern Oscillation Index (SOI). (a) Regional mean change in log relative risk (β_{SOI}) of hurricane frequency per SD (b) Same, but for the SDs. (c) Regional change in relative risk (β_{SOI}) of hurricane frequency per one SD increase in SOI, conditional upon holding all other covariates constant. Positive values (*red*) indicate regions where more storms are predicted when the SOI is high. Negative values (*blue*) indicate regions where more storms are predicted when the SOI is low (none qualifying). Hexagon regions where <10 % of β_{SOI} samples are below (or above) zero are outlined in *black*. (d) Histogram of β_{SOI} for region W. (e) The same, but for region E.

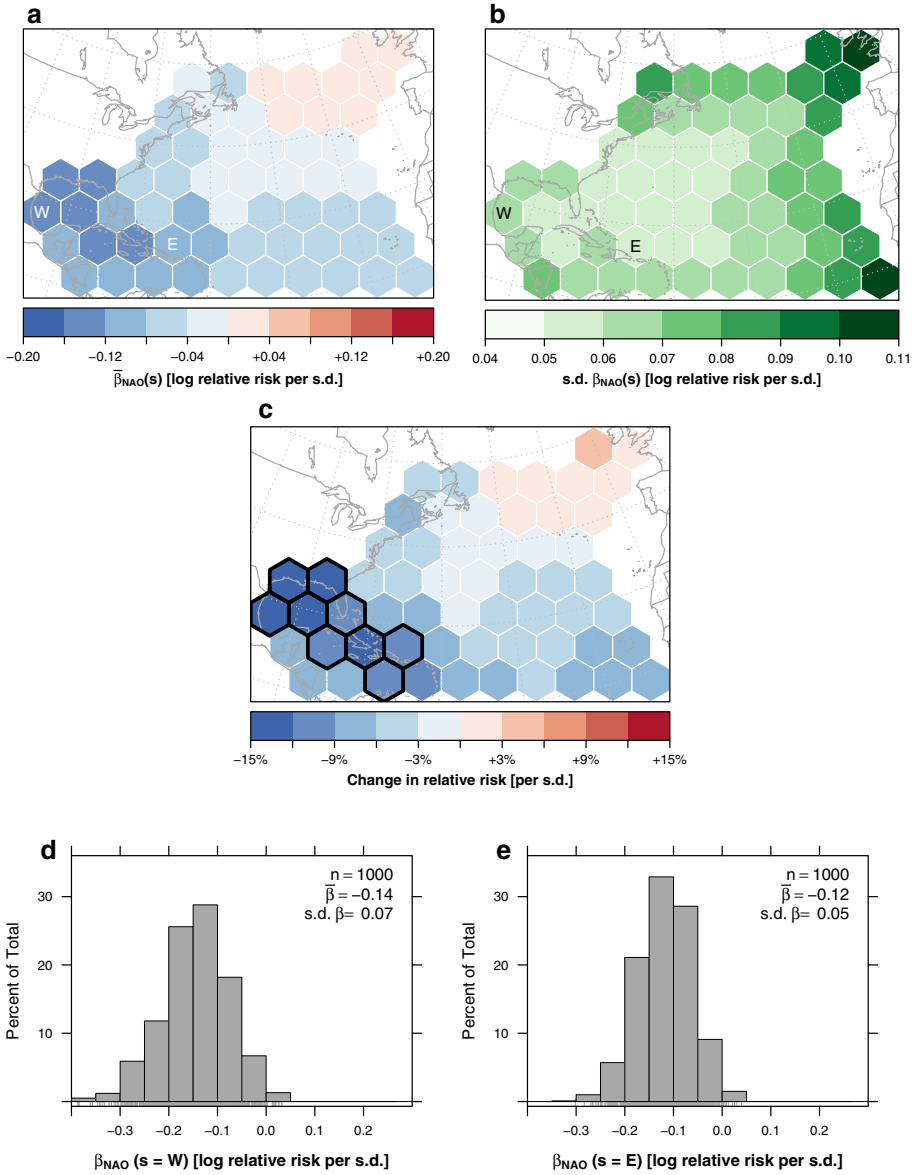

Fig. 7 Space–time model output for the North Atlantic Oscillation (NAO). (a) Regional mean change in log relative risk (β_{NAO}) of hurricane frequency per SD (b) Same, but for the SD. (c) Regional change in relative risk (β_{NAO}) of hurricane frequency per one SD increase in the NAO, conditional upon holding all other covariates constant. Positive values (*red*) indicate regions where more storms are predicted when the NAO index is high. Negative values (*blue*) indicate regions where more storms are predicted when the NAO index is low. Hexagon regions where <10 % of β_{NAO} samples are below (or above) zero are outlined in *black*. (d) Histogram of β_{NAO} for region W. (e) The same, but for region E.

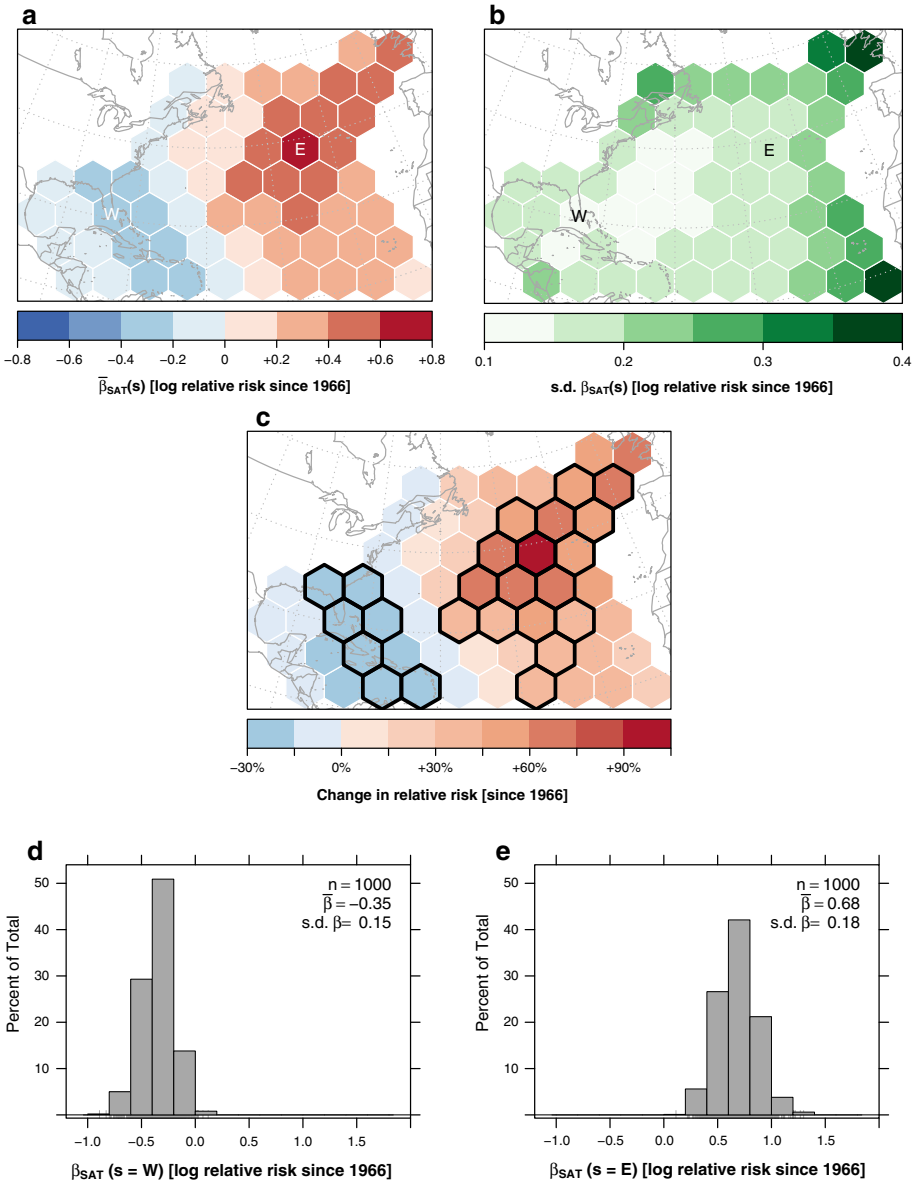

Fig. 8 Space–time model output for the indicator variable identifying seasons since 1966. (a) Regional mean change in log relative risk (β_{SAT}) of hurricane frequency since 1966. (b) Same, but for the SD. (c) Regional change in relative risk (β_{SAT}) of hurricane frequency since 1966, conditional upon holding all other covariates constant. Positive values (*red*) indicate regions where more storms are predicted since 1966. Negative values (*blue*) indicate regions where fewer storms are predicted since 1966. Hexagon regions where <10 % of β_{SAT} samples are below (or above) zero are outlined in *black*. (d) Histogram of β_{SAT} for region W. (e) The same, but for region E.

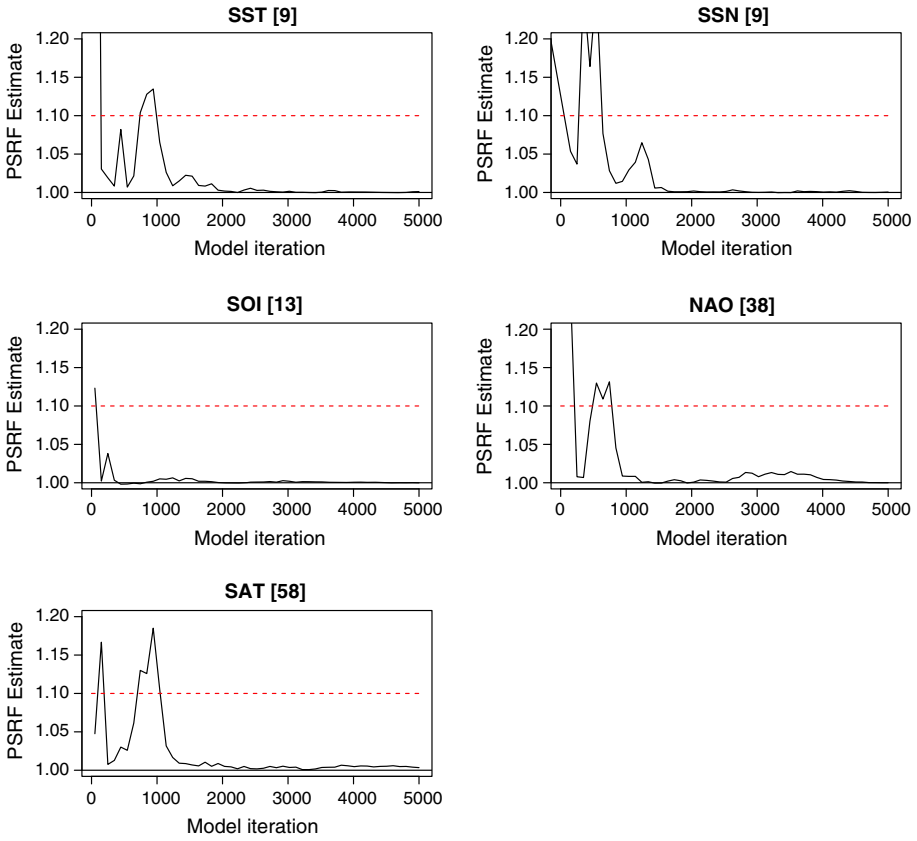

Fig. 9 Evolution of the potential scale reduction factor (PSRF) for select covariates and corresponding hexagon regions.

4.3 SOI

Log relative risks of annual hurricane frequency (Fig. 6a) range between +0.01 and +0.11 per SD over the basin. Values for Figs. 6d and e, regions located in the southwestern Caribbean and north-central tropical Atlantic, are +0.11 and +0.05, respectively.

Relative risks range between +1.4 and +11.5 % (Fig. 6c) over the basin. There are no significantly negative relative risk regions. The average relative risk over the thirty-four significantly positive regions is +7.8 % (SD 2.8 %).

4.4 NAO

Log relative risks of annual hurricane frequency (Fig. 7a) range between −0.14 and +0.03 per SD over the basin. Values for Figs. 7d and e, regions located in the western Gulf of Mexico and northern Antilles, are −0.14 and −0.11, respectively.

Relative risks range between −13.1 and +2.8 % (Fig. 7c) over the basin. The average relative risk over the eight significantly negative regions is −11.6 % with SD 1.3 %. There are no significantly positive regions.

4.5 SAT

Log relative risks of annual hurricane frequency (Fig. 8a) range between −0.34 and +0.68 since 1966 over the basin. Values for Figs. 8d and e, regions located in the southwestern Caribbean and north-central tropical Atlantic, are −0.19 and +0.43, respectively.

Relative risks range between −28.9 and +97.5 % (Fig. 8c) over the basin. The average relative risk over the four significantly negative regions is −26.5 % with SD 2.0 %. The average relative risk over the sixteen significantly positive regions is +56.7 % (SD 16.3 %).

5 Discussion

Here, we describe the model results by focusing on the effect of the covariates on regional hurricane frequency. We contrast the covariate response here against the current understanding of the relationship. We begin with sunspot numbers.

5.1 SSN

Consistent with earlier studies (EJ08 and HE12), the effect of SSN on hurricane frequency changes sign across the basin from west to east. The Atlantic basin is effectively split in half, with the eastern half indicating a beneficial effect of solar activity upon regional hurricane frequency, while the western half shows a detrimental effect.

Regions within the southwest Atlantic indicate a negative relationship. Reduced hurricane intensities in response to upper-level warming Elsner et al. (2010) are likely driving the frequency response in these regions. The statistical relationship shows that a moderate Category 1 hurricane (37.5 ms^{-1}) would decrease in intensity by approximately −4.5 ms^{-1} per 0.01 Mg II core-to-wing ratio units (SD), or 12 %. The linear relationship between daily sunspot number and the Mg II is quite strong Hodges and Elsner (2010), with an increase of 0.01 Mg II units corresponding to an increase in 104 sunspots. The 16–17 % reduction in hurricane likelihood for the southwest Atlantic from this study appears to match the 12 % reduction in intensity for this region. While there is a significant difference in study periods—1979–2007 versus 1866–2010—the detrimental effect, however, is consistent.

Note that none of the US Atlantic coastline is included in any significantly negative regions. However, the sign on the coefficient in these regions is all negative. It is reasonable to assume these signals correspond to fewer US seasonal hurricanes when the sun is active Elsner and Jagger (2008). HE12 constructed hurricane count differences per region by comparing the highest and lowest SSN hurricane seasons. The exclusion of roughly half the data in their approach may explain why their US East Coast patterns do not show up as statistically significant patterns shown here.

September sunspots have value as a “predictable” predictor. Solar cycle amplitudes and sunspot numbers maxima have shown predictability to within 20 % accuracy 30 months into the cycle, and within 10 % accuracy after 42 months Hathaway et al. (1994). Solar Cycle 24 began in January 2008, which—at the time of writing—means the cycle is over 60 months old. The Solar Physics Group at NASA’s Marshall Space Flight Center (http://solarscience.msfc.nasa.gov/predict.shtml) predict a peak of 69 sunspots for Sunspot Cycle 24 in the Fall of 2013. Assuming that value for September 2013 Bhatt et al. (2009), places

like southeastern Cuba, the southern Bahama islands, Haiti, Jamaica, and the Yucan Straits can expect approximately a 11.5 % lower probability of receiving a hurricane.

A new finding here is the location and magnitude of the southeast Atlantic response to SSN. Here, regions of enhanced hurricane activity extend further north ($\approx$40 N) and east ($\approx$20 E) than previously identified ($\approx$30 N; $\approx$20 E). However, the largest magnitudes from SSN reside in the south and southeast Atlantic. Given a season where SSN is 160 sunspots (the 95th percentile of 1866–2010 SSN), the risk of a hurricane in one southeast Atlantic region increases by almost 67 %.

A physical explanation for the east/west basin response is still unclear. Additional warming of the sea surface from increased solar activity White et al. (1997) in southeastern regions could lead to increased hurricane frequency. However, the SST response to solar activity appears marginal, with only a 0.05 °C change in global-average sea-surface temperature per 0.5 W m^{-2}. Consider that sunspots are significantly related to solar irradiance, with the equation relating the two variables as:

$$S = 1371.32 + (0.00734 \pm 0.00069)R_z \tag{7}$$

, where S is solar irradiance (W m^{-2}) and R_z is the Wolf Sunspot Number, a synonym for the International Sunspot Number used in this study [Hoyt and Schatten (1997) p. 61]. A value of 100 SSN, therefore, would correspond to a solar radiance increase of roughly 0.73 W m^{-2}. An increase of +0.73W m^{-2} would correspond to a +0.073 °C increase in SST. An increase in SST of this amount in the region of highest increase in relative risk per °C in Fig. 4c (i.e., the eighth region from bottom left to right) would produce a relative risk of roughly +7 %, far less than the observed increase in relative risk per 100 SSN of +40.9 % in the same region. In other words, the SSN influence on SST only explains about 17 % of observed increase in hurricane likelihood, clearly indicating there are other physical factors in play here.

An alternative explanation to the thermodynamic arguments of EJ08 could involve solar activity effects upon African Easterly Waves. Recent work by Loon and Meehl (2012) indicates a steeper Indian land-to-sea pressure gradient when sunspots are numerous. This leads to a more vigorous Findlater Jet, a low-level cross-equatorial flow that peaks in July during the southwest Indian Monsoon. Likewise, a more vigorous African Easterly Jet during periods of high solar activity could potentially lead to stronger African Easterly Waves—which account for almost 60 % of Saffir-Simpson category 1 and 2 hurricanes from 1967 to 1991 Landsea (1993). If so, it could explain the increase in hurricane frequency in the eastern Atlantic during high solar activity. Further study is required.

5.2 SST

The tropical Atlantic main development region demonstrates a positive relationship (red) to increased SST. More hurricanes are likely in genesis regions when seas are anomalously warm. Shapiro and Goldenberg (1998) previously discovered this relationship in the same areas, though their study used hurricane frequency from August to October and a non-spatial linear regression model to diagnose the response.

The northern and western Gulf of Mexico regions (from New Orleans, Louisiana through the Bay of Campeche) indicate a negative relationship. The relative risk for these regions are +32.0 and +30.1 %, respectively, when local SSTs are 1°C cooler than normal. While seemingly contrary to hurricane development, these peripheral regions—along with the two significant north Atlantic regions—may receive more hurricanes when other

regions are also cooler than normal. In this case, tropical waves may need longer to develop into hurricanes, leading to later-developing hurricanes into these regions.

5.3 SOI

During El Niño, stronger upper-level winds over the western Atlantic Arkin (1982) create an environment unfavorable for tropical cyclones, resulting in a decrease in hurricane frequency over the region Gray (1984). The positive (negative) relationship between La Niña (El Niño) conditions in these regions agrees with previous findings of fewer total storms Landsea et al. (1999) and fewer storms crossing the lower Caribbean during El Niño conditions Gray and Sheafer (1991). The relationship is strongest in the lowest latitudes and closest to the equatorial East Pacific, yet persists throughout most of the North Atlantic.

5.4 NAO

Much of the western tropical Atlantic—the lesser and greater Antilles and the Gulf of Mexico—show significantly lower probabilities of receiving a hurricane when the NAO is positive. A positive NAO pattern is defined as a stronger-than-normal pressure difference between the Icelandic low and North Atlantic subtropical high. The effective result is a northerly and easterly displacement of the North Atlantic subtropical high that steers fewer hurricanes into the Caribbean and Gulf regions Liu and Fearn (1999) and correlates to decreased US Gulf coast hurricane activity Elsner et al. (2000).

5.5 SAT

The increased risk in hurricanes since 1966 in the eastern Atlantic basin results may be explained by the undercounting of hurricanes that recurve and go unobserved prior to the advent of open-ocean satellite coverage Landsea et al. (2004), or a shift in hurricane climate—such as more (less) hurricanes in the northeast (southwest) Atlantic—since 1966. Results here affirm the spatial pattern noted by Vecchi and Knutson (2011), which indicate a west/east split at 62.5 °W of fewer and more hurricanes, respectively.

5.6 Further discussion

All of the individual climate factors (SST, SOI, NAO, SAT) known to impact North Atlantic hurricanes support the original findings discovered by previous investigators. This adds to the credibility of the space–time model output with respect to the SSN regional responses.

We can quantify the spatial extent of each climate factor. We do this by comparing the percentage of regions deemed significant according to the 90 % credible interval on coefficients.

The SOI impact on regional hurricane frequency displays the greatest spatial extent over the study area with 32 of 59 regions reporting a significant relationship, or roughly 54.2 % of the Atlantic basin. This constitutes an area of over 17 million km^2, or approximately the area of South America, and includes areas comprising the entire US Atlantic coastline with the exception of the extreme northeast.

The SAT covariate displays the second greatest spatial coverage of significant regions at 24 (40.1 %). SST and SSN covariates display the third greatest spatial coverage of

significant regions 21 (33.9 %) of 59 regions. The NAO covariates 9 (15.3 %) significant areas over the mapped basin, respectively.

Out space–time model tells us that SOI is spatially the most dominant climatologic factor toward describing regional hurricane frequency. It spans 14.1 % more area of the Atlantic basin than SAT, 20.3 % more than SST or SSN, and 38.9 % more than the NAO. Note that SSN impact on hurricanes affects more than twice the basin area than that of the NAO.

The significant SOI and NAO areal impacts do not change sign and are predominantly western basin phenomena. Conversely, the response in hurricane frequency from SST is primarily a homogeneous southeast Atlantic phenomenon. SAT and SSN both feature a split-basin heterogeneous response.

6 Summary

Here, we use a space–time model to examine the regional frequency of hurricanes in response to September sunspots while controlling for other relevant climate factors. A spatially coherent pattern emerges that features fewer (more) hurricanes across the Caribbean during high (low) sunspot years, affirming the intensity and count patterns described in EJ08 and HE12. The finding is consistent with EJ08 who identified a statistically significant solar activity signal in US-affecting hurricane frequency using SSN as a covariate. Though not statistically significant, an East Coast response similar to that found in the Caribbean is indicated by the space–time model. Now here is an increase in southeastern Atlantic hurricanes in response to higher SSN at almost three times the rate of decreased counts in the southeast Atlantic.

The model can be ported to explore other spatio-statistical relationships over contiguous space. It is worth noting the standard statistics caveats that one must be cautious when interpreting regression coefficients from these models, even in the context of models that incorporate spatial dependence Hughes and Haran (2012), Reich et al. (2006).

From a computational perspective, improvements include an alternative approach to the MCMC sampling performed herein. Integrated nested Laplace approximation (INLA) can be used to arrive at posterior marginals while alleviating the computational burdens and convergence issues that can interfere with MCMC methods Rue and Martino (2009).

References

Allan R, Nicholls N, Jones P, Butterworth I (1991) A further extension of the Tahiti-Darwin SOI, early SOI results and Darwin pressure. J Clim 4:743–749

Arkin P (1982) The relationship between interannual variability in the 200mb tropical wind field and the Southern Oscillation. Mon Weather Rev 110:1393–1404

Berliner L (1996) Hierarchical Bayesian time series models. In: Hanson K, Silver R (eds) Maximum entropy and Bayesian methods. Kluwer Academy, Dordrecht

Besag J, York J, Mollie A (1991) Bayesian image restoration, with two applications in spatial statistics. Ann Inst Stat Math 43:1–59

Bhatt N, Jain R, Aggarwal M (2009) Prediction of the maximum amplitude and timing of sunspot cycle 24. Sol Phys 260:225–232

Cohen T, Sweetser E (1975) The 'spectra' of the solar cycle and of data for Atlantic tropical cyclones. Nature 256:295–296

Elsner J, Hodges R, Jagger T (2011) Spatial grids for hurricane climate research. Clim Dyn 39:21–36

Elsner J, Jagger T (2008) United States and Caribbean tropical cyclone activity related to the solar cycle. Geophys Res Lett 35:L18,705

Elsner J, Jagger T (2013) Hurricane climatology: a modern statistical approach using R. Oxford University Press, Oxford
Elsner J, Jagger T, Dickinson M, Rowe D (2008) Improving multiseason forecasts of North Atlantic hurricane activity. J Appl Meteorol Climatol 21:1209–1219
Elsner J, Jagger T, Hodges R (2010) Daily tropical cyclone intensity response to solar ultraviolet radiation. Geophys Res Lett 37:L09,701
Elsner J, Kocher B (2000) Global tropical cyclone activity: a link to the North Atlantic Oscillation. Geophys Res Lett 27:129–132
Elsner J, Liu K, Kocher B (2000) Spatial variations in major US hurricane activity: statistics and a physical mechanism. J Clim 13:2293–2305
Emanuel K (1987) The dependence of hurricane intensity on climate. Nature 326:483
Emanuel K, Solomon S, Follini D, Davis S, Cagnazzo C (2013) Influence of tropical tropopause layer cooling on Atlantic hurricane activity. J Clim
Gelman A, Hill J (2007) Data analysis using regression and multilevel/hierarchical odels. Cambridge University Press, Cambridge
Gelman A, Rubin D (1992) Inference from iterative simulation using multiple sequences. Stat Sci 7:457–472
Gilks W, Richardson S, Spiegelhalter DJ (eds) (1996) Markov chain monte carlo in practice. Chapman and Hall, London, p 486
Gray W, Sheafer J (1991) El Niño and QBO influences on tropical cyclone activity. In: Glantz MH, Katz RW, Nicholls N (eds) Teleconnections linking worldwide climate anomalies. Cambridge University Press, Cambridge
Gray WM (1984) Atlantic seasonal hurricane frequency: 1. El Niño and 30-mb Quasi-Biennial Oscillation influences. Mon Weather Rev 112(9):1649–1668
Hathaway D, Wilson R, Reichmann E (1994) The shape of the sunspot cycle. Sol Phys 151:177–190
Hodges R, Elsner J (2010) Evidence linking solar variability with US hurricanes. Int J Climatol 31:1897–1907
Hodges R, Elsner J (2012) The spatial pattern of the sun-hurricane connection across the North Atlantic. ISRN Meteorol 2012:1–9
Hood L (2003) Thermal response of the tropical tropopause region to solar ultraviolet variations. J Geophys Res 30:2215–2225
Hoyt D, Schatten K (1997) The role of the sun in climate change. Oxford University Press, Oxford
Hughes J, Haran M (2012) Dimension reduction and alleviation of confounding for spatial generalized linear mixed models. J R Stat Soc Series B 75:139–159
Hurrell J, van Loon H (1997) Decadal variations in climate associated with the North Atlantic Oscillation. Clim Changes 36:301–326
Jagger T, Elsner J (2006) Climatology models for extreme hurricane winds near the United States. J. Clim. 19:3220–3236
Jarvinen, B.R., Neumann, C.J., Davis, M.A.S.: A tropical cyclone data tape for the north atlantic basin, 1886–1983: Contents, limitations, and uses. Technical Memo. 22, NOAA NWS NHC (1984)
Können G, Jones P, Kaltofen M, Allan R (1998) Pre-1866 extensions of the Southern Oscillation Index using early Indonesian and Tahitian meteorological readings. J Clim 11:2325–2339
Labitzke K, Austin J, Butchart N, Knight J, Takahashi M, Nakamoto M, Nagashima T, Haigh J, Williams V (2002) The global signal of the 11-year solar cycle in the stratosphere: observations and models. J Atmospheric Sol Terr Phys 64:203–210
Landsea C (1993) A climatology of intense (or major) Atlantic hurricanes. Mon Weather Rev 121:1703–1713
Landsea C, Anderson C, Charles N, Clark G, Dunion J, Partagas J, Hungerford P, Neumann C, Zimmer M (2004) The Atlantic hurricane database re-analysis project: Documentation for the 1851–1910 alterations and additions to the HURDAT database. In: Murnane R, Liu KB (eds) Hurricanes and Typhoons: Past, Present and Future. Columbia University Press, Columbia, pp 177–221
Landsea C, Pielke RW Jr, Mesta-Nuñez A, Knaff J (1999) Atlantic basin hurricanes: indices of climatic changes. Clim Changes 42:89–129
Liu K, Fearn M (1999) Reconstruction of prehistoric landfall frequencies of catastrophic hurricanes in northwest Florida from lake sediment records. Quat Res 54:238–245
Mann M, Park J (1994) Global-scale modes of surface temperature variability on interannual to century timescales. J Geophys Res 99:25,819–25,833
Meldrum C (1872) On a periodicity in the frequency of cyclones in the Indian Ocean south of the equator. Nature 6:357–358

Neumann, C., Jarvinen, B.R., McAdie, C.J., Hammer, G.R.: Tropical Cyclones of the North Atlantic Ocean, 1871–1999. Historical Climatology Series 6–2, National Environmental Satellite, Data, and Information Service, Asheville, North Carolina (1999)
Plummer M, Best N, Cowles K, Vines K (2006) CODA: convergence diagnosis and output analysis for MCMC. R News 6:7–11
Poey A (1873) Sur les rapports entre les taches solaires et les ourages des Antilles de l'Atlantique-nord et de l'Ocean Indien sud. Compt Rend 77:1223–1226
Reich B, Hodges J, Zadnik V (2006) Effects of residual smoothing on the posterior of the fixed effects in disease-mapping models. Biometrics 62:1197–1206
Ropelewski C, Jones P (1987) An extension of the Tahiti-Darwin Southern Oscillation Index. Mon Weather Rev 115:2161–2165
Rue H, Martino S (2009) Approximate Bayesian inference for latent Gaussian models by using integrated nested Laplace approximations. J R Stat Soc B 71:319–392
Shapiro L, Goldenberg S (1998) Atlantic sea surface temperatures and tropical cyclone formation. J Clim 11:578–590
Shekhar S, Xiong H (eds) (2008) Encyclopedia of GIS. Springer, New York
Smith T, Reynolds R, Peterson TC, Lawrimore J (2008) Improvements to NOAA's historical merged land-ocean surface temperature analysis (1880–2006). J Clim 21:2283–2296
van Loon H, Meehl G (2012) The Indian summer monsoon during peaks in the 11 year sunspot cycle. Geophys Res Lett 39:L13,701
Vecchi G, Knutson T (2011) Estimating annual numbers of Atlantic hurricanes missing from the HURDAT database (1878–1965) using ship track density. J Clim 24:1736–1746
Visher S (1924) Sunspots and the frequency of tropical cyclones. Am J Sci 8:312–316
Weiss N (2007) Sunspot structure and dynamics. In: Baker D (ed) Solar dynamics and its effects on the heliosphere and Earth. Springer, New York, pp 13–22
White W, Lean J, Cayan D, Dettinger M (1997) Response of global upper ocean temperature to changing solar irradiance. J Geophys Res 102:3255–3266
Wikle C, Anderson C (2003) Climatological analysis of tornado counts using a hierarchical Bayesian spatiotemporal model. J Geophys Res 108:9005
Wikle C, Berliner L, Cressie N (1998) Hierarchical Bayesian space-time models. Environ Ecol Stat 5:117–154
Willett H (1951) Extrapolation of sunspot-climate relationships. J Meteor 8:1–6